



Reduced graphene oxide coated graphite electrodes for treating Reactive Turquoise Blue 21 rinse water using an indirect electro-oxidation process

Naresh R. Vaghela¹ · Kaushik Nath²Received: 27 August 2020 / Accepted: 14 October 2020 / Published online: 18 October 2020
© Springer Nature Switzerland AG 2020

Abstract

The present study deals with the decolourization of synthetic Reactive Turquoise Blue 21 (RTB21) dye-based model wastewater using an indirect electro-oxidation process and enhanced by modified graphite electrodes. Graphene oxide (GO) was successfully synthesized and deposited on the surface of pre-treated graphite electrodes. It was further reduced to form reduced graphene oxide (rGO). The resultant newly developed anode electrodes were designated as (Gr)₀, (rGO/Gr)₁, and (rGO/Gr)₂ and used for the treatment of wastewater. Electrodes, thus developed, were characterized using Fourier-transform infrared spectroscopy, X-ray diffractions, Field emission scanning electron microscopy, and Contact angle (CA). The effect of process parameters such as initial pH, current density, electrolyte concentration, and temperature on the performance of novel anode electrodes was investigated. The colour removal efficiency was increased significantly almost 25.80% in the presence of a modified electrode with the highest efficiencies of about 96.69% in a natural pH environment, 200 A/m², 2 g/L NaCl concentration, 30 °C temperature, and 15 min process time for 50 ppm RTB21 dye concentration for (rGO/Gr)₂ electrode. The RTB21 decolourization by indirect electro-oxidation process follows the pseudo-first-order kinetics, and the activation energy was estimated to be 23.42 kJ/mol. The stability of (rGO/Gr)₂ electrode was also examined. The rGO coated electrode was a superior electrode for the indirect electro-oxidation process, giving enhanced colour removal (%).

Keywords Graphene oxide · Reduced graphene oxide · Wastewater · Indirect electro-oxidation process

1 Introduction

Discharge of rinse water associated with industrial dyeing operations poses a serious challenge towards its efficient reclamation. Annually 280,000 tons dyes are discharged into water bodies worldwide, out of which around 8000 tons comprise of reactive dyes with extremely high colour fastness, chemical stability, and resistance towards oxidation. Several physico-chemical methods for treating dye wastewater are available; however, most of these systems seem to be plagued with low practical efficiency

or low benefit–cost ratio. Common wastewater treatment techniques include adsorption [1], chemical coagulation [2], electrocoagulation [3], biological process [4], Fenton process [5], membrane filtration [6], and so on. But the issues of disposal of copious amounts of coloured sludge, membrane fouling, regeneration of spent adsorbents, equilibrium limitation, and many others render most of these processes unfeasible options. Another key problem with most of the approaches mentioned earlier is versatility for removing all classes of dyes. Adsorption suffers from expensive adsorbent regeneration, long treatment

✉ Kaushik Nath, drkaushiknath2013@gmail.com | ¹Department of Chemical Engineering, Government Engineering College (Affiliated To Gujarat Technological University, Ahmedabad), Bharuch 392002, Gujarat, India. ²Department of Chemical Engineering, G.H.Patel College of Engineering & Technology, Vallabh Vidyanagar 388120, Gujarat, India.



time, and solid disposal issues, despite being effective for treating dye-containing effluent [7]. Chemical coagulation could attain a high removal efficiency, but it produces a large quantity of subsequent wastewater, which needs further treatment leading to overall high processing cost [8]. Fenton like processes and electrocoagulation produces a significant amount of sludge and is not effective for complete degradation of dye molecules. Membrane processes are capable of separation of almost all types of dyes from the effluent. There is no sludge formation, and the space requirement is also less. But the high cost of membrane and equipment, fouling problems during operation, are the limitations of the membrane process [9]. Biological treatment is economical, ineffective in the treatment of refractory organic wastewater [8]. Therefore, complete destruction of dye molecules from synthetic wastewater is an urgent need considering ecology and environmental damage prevention. It requires effective and eco-friendly techniques with high removal efficiency and low cost.

Of late electrochemical processes, particularly indirect electro-oxidation (EO) or direct anodic oxidation (DAO) process has drawn considerable attention for the reclamation of industrial wastewater [10, 11]. Electrochemical methods neither produce sludge nor require a substantial amount of chemicals. Additionally, the processes are operated at ambient conditions [12]. Adsorption of pollutants at the electrode surface, followed by their complete degradation into CO_2 and H_2O by electron transfer reaction, could be achieved in DAO [13]. On the other hand, in EO, a reactive oxidizing agent like HOCl/Cl_2 , H_2O_2 , and ozone generated in situ due to redox reaction tends to degrade the pollutant in bulk the solution [12].

The variety of processing parameters reported in the literature and the complexity of the mechanisms associated with electro-oxidation in dye wastewater treatment is yet scientifically elucidated. This underscores a very perceptible need for more research for an improved method, system, and apparatus for treating wastewater over the existing art. The material of construction, shape, and size of the electrodes constitutes a key research area in the electro-oxidation process. The carbonaceous materials have been extensively studied for electro-oxidation methods due to their exceptional electrocatalytic activity, high chemical stability, and superior conductivity. Graphite electrodes are frequently used as anode and cathode electrode for their commercial availability, unique electrocatalytic activity, and nontoxicity to degrade dyes [14].

The graphite electrode surface can be modified to enhance electrical conductivity by different materials, metal-based oxides, polymers, and carbon-based materials [15–17]. Graphene oxide (GO) and reduced graphene oxide (rGO) are widely acknowledged as effective coating materials on account of their exceptional characteristics,

such as high specific surface area, electric conductivity, and good chemical stability [18, 19]. GO or rGO can be used as modification materials for electrochemical sensors [20–23]. However, a perusal of recent literature indicates that most of the research on GO or rGO coating over graphite electrode has been focused on Electro Fenton (EF) process, specifically decisive on cathode modification. Akerdi et al. [18] investigated the performance of the EF process using the GO and rGO coated Graphite electrode for decolourization of Methylene Blue (MB) and Acid Red 14 (AR14). Zhang et al. [24] demonstrated that graphene@graphite-based gas diffusion electrode (G-GDE) as an efficient and low-cost cathode material for the EF process. Bondarenko et al. [15] fabricated the SnO_2/rGO composite film electrode shows high electrocatalytic activity for anodic oxidation of organic and inorganic substances. To the best of our knowledge, rGO modified graphite electrode as the anode is being reported for the first time to degrade the Reactive Turquoise Blue 21 (RTB21) from a model dye wastewater by the indirect electro-oxidation process. The RTB21 is widely used in the textile industry due to its unsurpassed qualities like incomparable stability, optimum solubility, and longer shelf life. It is difficult to degrade the RTB21 dye because of its highly stable aromatic structure. The discharge of RTB21 dye into water bodies from various textile industries becomes a grave concern due to their non-biodegradability, toxicity, and mutagenicity. Thus, it is damaging to the aesthetic value of the environment [25].

Keeping these into consideration, the present study aims at the facile synthesis of rGO coated electrode for the removal of RTB21 dye by the electro-oxidation process. GO was synthesized using improved Hummer's method. Firstly, GO was coated on a graphite electrode than reduced to rGO using the thermal method. The effect of process parameters such as initial pH, current density, electrolyte concentration, and temperature on colour removal efficiency of dye was also studied using the graphite and rGO coated graphite electrode as anode and graphite electrode as the cathode. Besides, physical characterization was carried out by X-ray diffraction (XRD), Field emission scanning electron microscopy (FESEM), and contact angle (CA) techniques to study the electrode performance, as well as its stability. The work presented herein, although exploratory in nature, sought to provide new insights into wastewater treatment of the textile, dyestuff industry and to supplement the information on clean technology.

2 Materials and method

2.1 Chemicals and materials

The textile dye Reactive Turquoise Blue 21, used in the present study, was procured from M/s Snehal Dye Chem. Ltd, Ankleshwar, Gujarat, India. The dye was used without any further treatment. The general characteristics of the dye are given in Table 1. All other chemicals (AR grade) were obtained from Merck, India and were used without any additional purification. Deionized (DI) water (conductivity $\sim 1 \mu\text{S}/\text{cm}$) was used during synthesis and other experiments. Natural Graphite flakes were purchased from Mass Graphite and Carbon Products, Gujarat, India. Graphite electrode ($3 \times 2 \times 0.20 \text{ cm}$) was provided by Prime Industries, Maharashtra, India, and was used as a substrate for GO coating and electrode in the dye removal process.

2.2 Synthesis of GO

Graphite flakes were oxidized following improved Hummer's method to synthesize GO. 3.0 g of graphite flakes were added slowly to a mixture of 360 mL concentrated H_2SO_4 , 40 mL H_3PO_4 , and 19 g KMnO_4 . During the mixing reaction, the temperature was kept below 20°C . The reaction mixture was stirred for 12 h with heating at 50°C . After cooling down to room temperature, the reaction mixture was poured into 400 mL ice followed by the addition of 2 mL, 30% H_2O_2 to remove unreacted KMnO_4 . After filtration of the reaction mixture, the filtrate was centrifuged at 400 rpm for 4 h, and the supernatant was decanted away. The solid material obtained from the centrifugation process was washed with DI water, 30% HCl and ethanol repeatedly for several times to remove dissolved impurities. The solid material was further centrifuged at 4000 rpm for 4 h, and the supernatant was decanted away. The remaining solid material was coagulated with 200 mL of ether. The suspension was filtered on Whatman paper,

and the residue was dried at ambient temperature under vacuum condition. Finally, approximately 5.8 g GO was obtained.

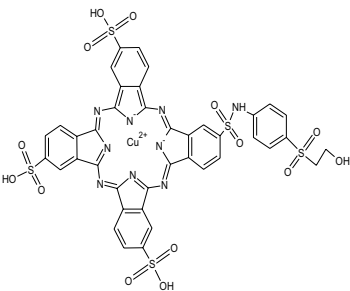
2.3 Preparation of GO dispersion and rGO coating over graphite electrode

To obtain homogenous suspension of GO in water, 0.1 g GO was added into 100 mL DI water followed by 3 h sonication (240 W) with continuous stirring. Graphite electrode surfaces were pre-treated prior to coating. Pre-treatment was carried out by dipping the electrode into a dilute HCl solution for 2 h, followed by sonication (130 W) with acetone for 2 h. Finally, it was rinsed with DI water and was dried at 60°C for 24 h. The pre-treated graphite electrode, thus obtained, was denoted as raw Gr. The dip-coating method was used for the coating of GO over the graphite substrate. The raw Gr was dipped into a homogeneous suspension of GO under the continuous stirring condition for 3–5 s and dried for 30 min at 110°C in a hot air oven. This dipping cycle was repeated several times to ensure a significant coating of GO over raw Gr. Three sets of anode electrodes, namely uncoated Gr: $(\text{Gr})_0$, Gr with 10 cycles of GO coating: $(\text{GO}/\text{Gr})_1$ and Gr with 20 cycles of GO coating: $(\text{GO}/\text{Gr})_2$ were selected for the present study. GO reduction was carried out by the thermal reduction method. GO/Gr electrode was placed into the tubular furnace at 450°C for 60 min. These electrodes were designated as $(\text{Gr})_0$, $(\text{rGO}/\text{Gr})_1$, $(\text{rGO}/\text{Gr})_2$. Chemical structures of graphite, GO, rGO are presented in Fig. 1.

2.4 Electrochemical experiments

The indirect electro-oxidation process for the decolourization of RTB21 wastewater was carried out in an electrochemical cell schematically represented in Fig. 2. The electrochemical cell was made up of 250 mL cylindrical glass vessel. A total of 250 mL of RTB21 dye wastewater was taken for each set of experiments, and the same was carried out in

Table 1 Characteristics of treated dye

Chemical structure	Molecular formula	Colour index name	λ_{max} (nm)	Molecular weight (g/mol)
	$\text{C}_{40}\text{H}_{25}\text{CuN}_9\text{O}_{14}\text{S}_5$	C.I. Reactive Blue 21	624	1159.62

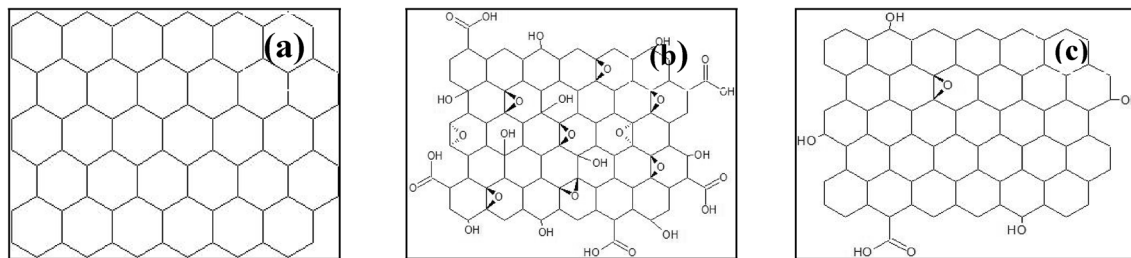


Fig. 1 Chemical structure of graphite (a), GO (b), rGO (c)

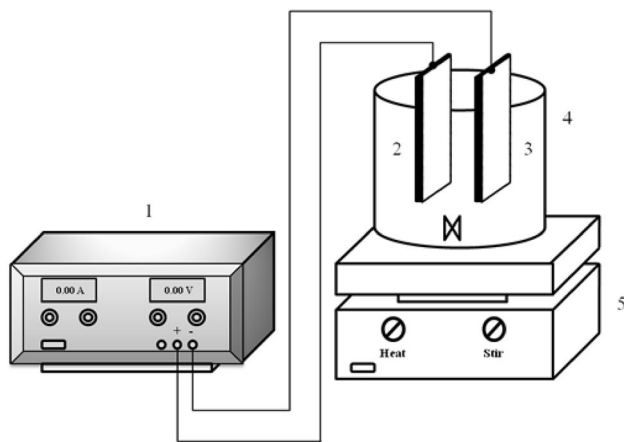


Fig. 2 Schematic diagram of the experimental set-up: (1) DC Power Supply, (2) Anode electrode, (3) Cathode electrode, (4) Electrochemical cell, (5) Magnetic stirrer

batch operation, continuously stirred by the magnetic stirrer at 800 rpm. Two plates of the electrode were used as anode and cathode for the electrochemical process. The anode was configured in a monopolar connection mode with cathode with an inter-electrode gap of 1 cm between the two plates. The effective area of the anode electrode was estimated to be 10 cm². Initial pH of the solution was adjusted by adding 0.1 M H₂SO₄ or 0.1 M NaOH and was measured by a digital pH meter (EI, Model no 112). A predetermined amount of NaCl was added to improve the conductivity before the Direct current (DC) supplied. The conductivity of the samples was measured by a digital conductivity meter (EI, model no. 651). The required current density (A/m²) was adjusted by regulating the voltage of DC regulated power supply (Make: SIGMA, 0–30 V 0–5 A). The colour removal efficiency of the sample collected at various time intervals was calculated using Eq. 1:

$$\text{Colour removal(\%)} = \left(1 - \frac{A}{A_0}\right) \times 100 \tag{1}$$

where, A_0 and A are the light absorbance of a sample before and after the electrochemical process, respectively, measured using a UV/VIS spectrophotometer (Model CL 335). The electrical energy consumption (C_{energy} , kWh/m³) for the EO process was determined according to Eq. 2 [26]:

$$C_{\text{energy}} = \frac{(Uit_{\text{EO}})}{v} \tag{2}$$

where U is the average cell voltage (V), i is the current (A), t_{EO} is the processing time (h), and v is the volume of the solution (m³). The current efficiency (CE) for the EO process was calculated using Eq. (3) [27].

$$\text{CE(\%)} = \frac{3.6nFv\Delta C}{it_{\text{EO}}} \times 100 \tag{3}$$

where n is the number of exchanged electrons, F is Faraday’s constant (96,487 C/mol), ΔC is the concentration difference of dye (mol/L). Samples collected at various time intervals were filtered through Whatman filter paper to remove the unwanted particulate matter present in a sample. RTB21 removal was studied by varying the specific parameter, keeping the other parameters constant, and the effect of various vital parameters was obtained. After each run, electrodes were washed by 0.1 M HCl solution to remove the organic impurities and oxide layer from electrodes and then dried for reuse.

The kinetic parameter for the EO process can be described by the Arrhenius equation as follows:

$$K_1 = Ae^{\left(\frac{-E_a}{RT}\right)} \tag{4}$$

where K_1 is the rate constant, A is the Arrhenius constant, E_a is apparent activation energy (kJ/mol), R is the ideal gas constant (0.0083 kJ/mol K), and T is the Temperature (K).

2.5 Characterization of rGO coating over graphite

The organic functional groups (chemical bonds) present in the sample were identified by the Fourier transform infrared spectroscopy (FTIR, Make: Shimadzu, IRPrestige-21).

The spectral outputs were recorded in the transmittance mode at the mid-infrared region of 4000–400 cm^{-1} as a function of wavenumber at a resolution of 4.0 cm^{-1} with an acquisition time of 1 min. The samples were kept under constant nitrogen flow at a rate of 10 mL min^{-1} to eliminate undesired absorbance by surrounding moisture and carbon dioxide. The electrodes' surface morphology was studied by field emission scanning electron microscopy (FE-SEM, Make: ESEM EDAX XL-30, Philips, Netherlands) at 10 kV. The diffraction patterns and the crystallinity of the synthesized materials were examined by D8 Advanced (Bruker, Germany) diffractometer with Cu K α radiation ($\lambda = 1.54 \text{ \AA}$) in the range $5^\circ \leq 2\theta \leq 85^\circ$. The X-ray generator (X-ray power 2 kW; detector: Xe-filled counterate) was operated at an excitation voltage of 45 kV and a current of 40 mA. The contact angle of water on synthesized material was examined by a contact angle meter Biolin Scientific (Model: Attention (Biolin Scientific) Theta). A 5- μL liquid was dropped using a micropipette on the material surface at room temperature.

3 Results and discussion

To accomplish a high level of efficiency for decolourization of RTB21 dye by EO process, several factors to be considered into accounts such as initial pH, current density (A/m^2), NaCl as an electrolyte concentration (g/L), and temperature ($^\circ\text{C}$). Optimum values find out to achieve a higher degree of decolourization considering all the experimental conditions.

3.1 Effect of initial pH

Initial pH plays a vital role in the performance of the EO process and is considered as one of the essential process parameters [28]. Thus, it is worthwhile to analyse the effect of the initial pH of feed solution on the colour removal efficiency in the presence of Gr and rGO coated Gr electrodes. In this work, the effect of the different initial pH (3.0–11.0) at process time 15 min for treatment of 50 ppm synthetic RTB21 wastewater was studied at 2 g/L NaCl, 200 A/m^2 current density, and 30 $^\circ\text{C}$ temperature. At acidic condition (3.0 pH), per cent colour removal was found to be 41.77, 54.11, and 62.17 for $(\text{Gr})_0$, $(\text{rGO/Gr})_1$, $(\text{rGO/Gr})_2$, respectively. At neutral pH, it was observed to be 73.37, 82.00, and 96.69 for $(\text{Gr})_0$, $(\text{rGO/Gr})_1$, and $(\text{rGO/Gr})_2$, respectively. Under the basic conditions, it was reduced compared to the neutral condition. Figure 3 presents the effect of initial pH on the experimental results of colour removal efficiency. However, the formation of active chlorine as a dominant oxidizing agent via the oxidation process at the anode could

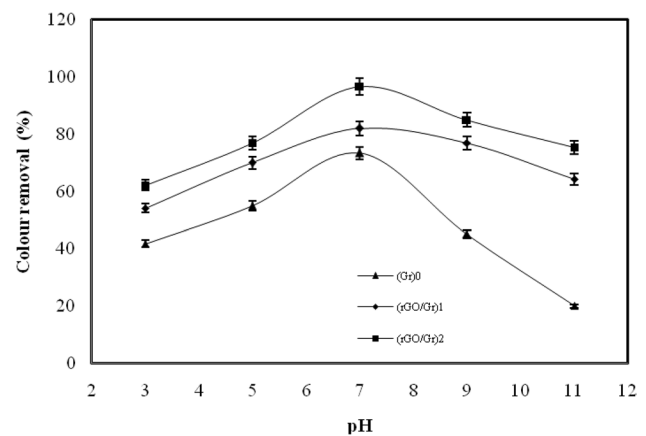
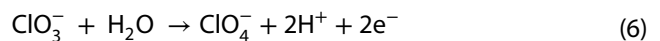
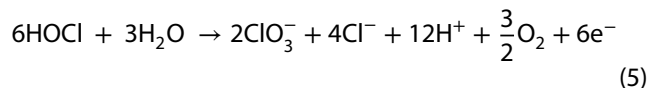


Fig. 3 Effect of Initial pH on colour removal (%) at constant 50 ppm dye concentration, 200 A/m^2 current density, 2.0 g/L NaCl concentration, 30 $^\circ\text{C}$ temperature, and 15 min process time

lead to the decolourization of RTB21 dye, which would be further reduced to HOCl or OCl^- [29].

In acidic conditions, relatively low stability the hypochlorous acid (HOCl) might be responsible for the reduced decolourization as HOCl possesses higher oxidation power (1.49 V) than that of OCl^- (0.94 V). On the other hand, in basic condition, chlorate or perchlorate productions from Cl_2/HOCl could lead to lower decolourization of RTB21 dye [13, 30], as shown by the chemical reactions (5) and (6):

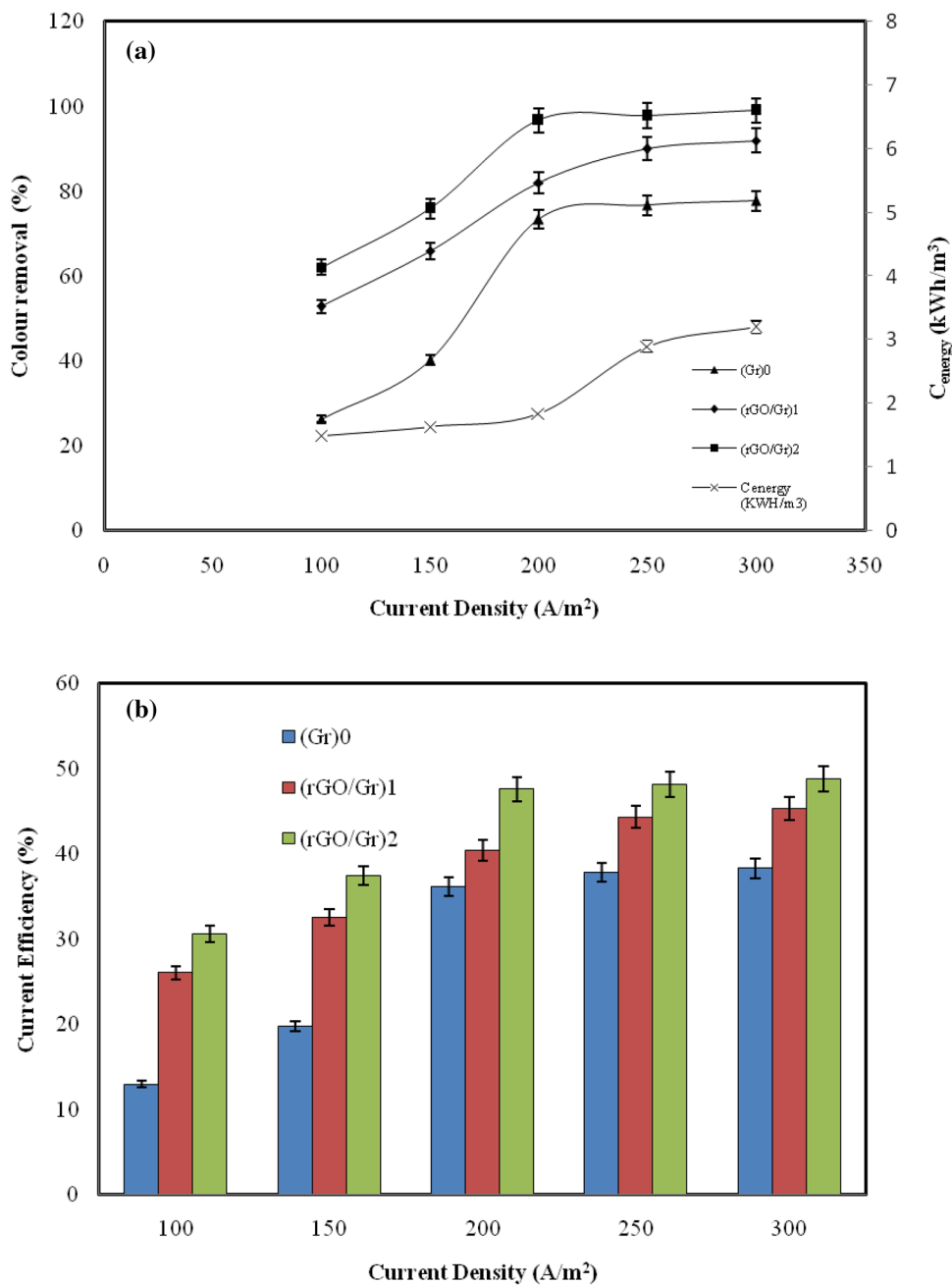


These results are in line with those obtained by Kariyajanavar et al. [31] and Rajkumar and Mathkumar [29].

3.2 Effect of current density

The reaction mechanism of EO is greatly influenced by current density—one of the most essential electrochemical process parameter. To analyse the effect of current density on the EO process of the present study, the current density in the range of 100–300 A/m^2 was applied by keeping other parameters constant at 7.0 initial pH, 30 $^\circ\text{C}$ temperature, 2 g/L NaCl, and 50 ppm synthetic RTB21 wastewater. Colour removal efficiency as a function of current density is presented in Fig. 4a. A perusal of Fig. 4a, reveals that the extent of colour removal efficiency increased with the increase in current density for all three electrodes. In the case of $(\text{Gr})_0$ electrode, the maximum per cent removal of colour was estimated to be 77.78%, while the same for $(\text{rGO/Gr})_1$ and $(\text{rGO/Gr})_2$

Fig. 4 Effect of current density (A/m^2) on colour removal (%) (a), current efficiency (%) (b) at constant 50 ppm dye concentration, 7.0 initial pH, 2.0 g/L NaCl concentration, 30 °C temperature, and 15 min process time



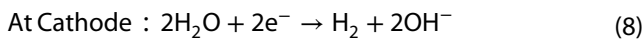
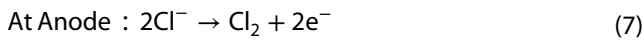
electrodes were 91.98% and 99%, respectively, at the current density of 300 A/m^2 . During the processing time of 15 min, electrical energy consumption increased from 1.5 to 3.2 kWh/m^3 . The per cent colour removal (%) could thus be improved by increasing the current density. It is worthwhile to note that as the current density was increased from 100 to 300 A/m^2 , the rate of generation of an oxidizing agent increased as well due to anodic oxidation thereby resulting in an improvement of the system efficiency [31, 32]. The relation between current efficiency and current density is presented in Fig. 4b

for all the three-electrode systems used in the present study. The results indicate that the current efficiency was almost constant after 200 A/m^2 irrespective of the nature of the graphite electrodes. However, it is imperative to mention that above 200 A/m^2 , no significant changes in the colour removal (%) could be achieved. It was plausibly because a part of the current devoured into an oxygen evolution reaction, besides oxidation of pollutants [33]. Hence, this was considered to be an optimum value for further experiments.

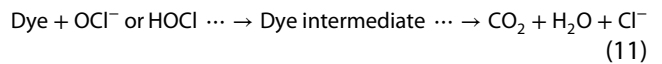
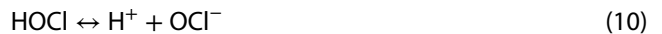
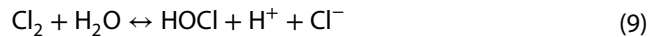
3.3 Effect of electrolyte concentration

A supporting electrolyte is added to the solution to improve the conductivity of the solution. The addition of electrolyte results in the reduction of electrical energy consumption and the ohmic drop. In the present work, NaCl was added as an electrolyte to improve the conductivity of the RTB21 wastewater to enhance the electron transfer rate between electrodes, thereby resulting in an enhancement in the decolourization of RTB21 dye. The experiments were conducted to determine the effect of NaCl concentration on the colour removal efficiency by EO process, for 50 ppm synthetic RTB21 wastewater in the range of 1–3 g/L NaCl concentration for 15 min keeping current density, initial pH, and temperature constant at 200 A/m², 7.0 and 30 °C, respectively, for all three electrodes used in the present study. The results are presented in Fig. 5. It reveals that the per cent colour removal of dyes for all the three-electrode systems increased with increasing NaCl concentration.

Moreover, it is observed that when NaCl concentration increased from 1 to 3 g/L, colour removal (%) achieved about 74.81, 85.00, and 97.37 for (Gr)₀, (rGO/Gr)₁, (rGO/Gr)₂, respectively. Besides, the conductivity of the solution increased significantly from 1452 to 3614 μS/cm, resulting in a reduction of the operating voltage from 18.1 to 7.1 V. Consequently, the electrical energy consumption reduced from 3.62 to 1.42 kWh/m³, and the electro-oxidation process was promoted by producing active chlorine at anode [30]. The mechanistic equations for the indirect electro-oxidation process are presented in Eq. (7–11) [12, 34],



In Bulk of the Solution:

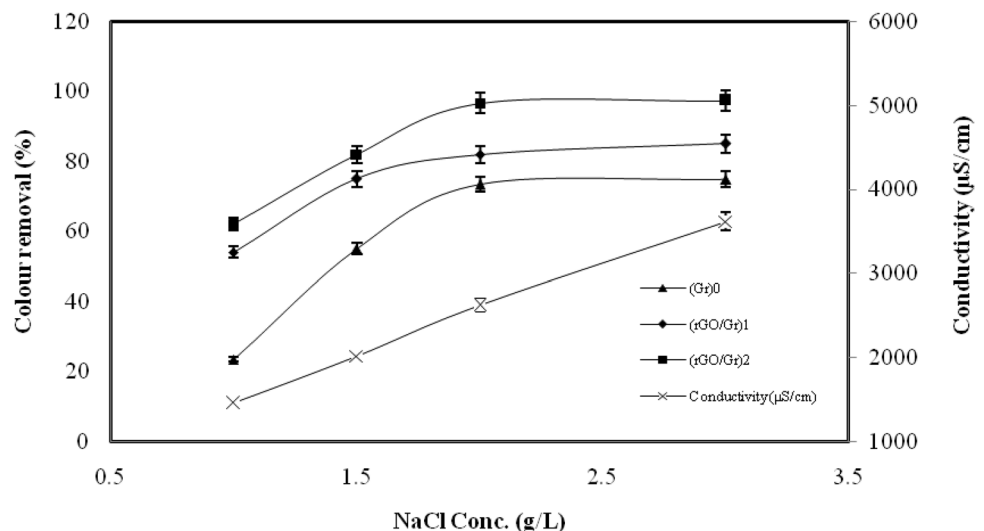


Enhancement in the NaCl concentration up to 2 g/L led to an increase in the extent of decolourization, and the same was almost 73.37, 82.00, and 96.69 (%) for (Gr)₀, (rGO/Gr)₁, (rGO/Gr)₂, respectively. This could be due to the generation of a more oxidizing agent such as Cl₂, HOCl, OCl⁻ [13] in the process. Therefore, 2 g/L NaCl concentration was considered to be optimal for successive degradation experiments.

3.4 Effect of temperature and thermodynamic study

The effect of temperature for 50 ppm synthetic RTB21 wastewater on colour removal (%) for the EO process was studied at four different temperatures (20, 30, 40, 50 °C) for all the three types of electrode keeping the other parameters (duration:15 min; current density: 200 A/m²; initial pH: 7.0, and NaCl concentration: 2 g/L) constant. As presented in Fig. 6, the results indicate that per cent colour removal increased with increase in temperature. It was observed that the per cent colour removal observed in (rGO/Gr)₂ electrode was higher than its two other counterparts. An increase in temperature could enhance the reaction rate between oxidants and dye, facilitating colour removal (%) in the EO process. But the high temperature could also enhance the decomposition rate of oxidants [35].

Fig. 5 Effect of NaCl concentration (g/L) on colour removal (%) at constant 50 ppm dye concentration, 7.0 initial pH, 200 A/m² current density, 30 °C temperature, and 15 min process time



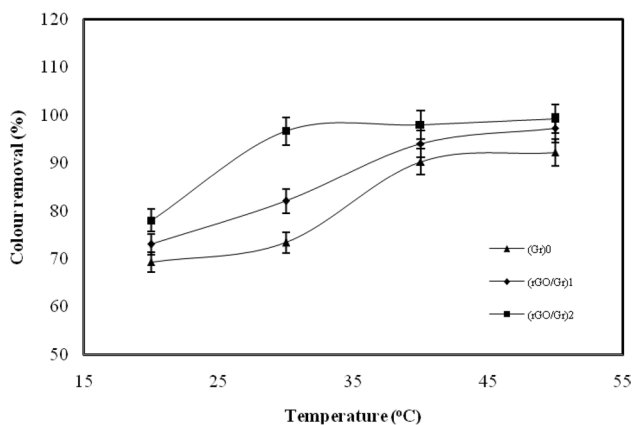


Fig. 6 Effect of Temperature (°C) on colour removal (%) at constant 50 ppm dye concentration, 7.0 initial pH, 200 A/m² current density, 2.0 g/L NaCl concentration, and 15 min process time

Therefore, the experiment temperature condition should not be kept too high. Similar observations are reported by Duan et al. [35]. The colour removal rate depends on dye concentration and the concentration of chlorine/hypochlorite. Therefore, the kinetics of colour removal was studied following Eq. (12)

$$d[C_t]/dt = k [C_t] [Cl_2] \tag{12}$$

where C_t is the concentration of RTB21 dye at time t , k is the first-order rate constant. In the EO process, chloride from wastewater gets converted into chlorine/hypochlorite. Oxidation of dye is carried out by chlorine/hypochlorite, the bulk solution, and then it is reduced back to chloride ion [30, 36]. Catalytically, the EO process repeats its behaviour. Therefore, during the experimental run, the concentration of chlorine/hypochlorite was assumed to be constant. Accordingly, Eq. (12) could be modified by a pseudo-first-order kinetic equation is as shown in Eqs. (13) and (14),

$$d[C_t]/dt = K_1 [C_t] \tag{13}$$

$$\ln \left(\frac{C_t}{C_0} \right) = -K_1 t \tag{14}$$

where C_0 is the initial dye concentration, K_1 is the apparent pseudo-first-order rate constant. The rate constant K_1 , min⁻¹, and respective R^2 value obtained from the slope of the plot of $\ln(C_t/C_0)$ versus time, shown in Table 2.

The Arrhenius plot of $\ln(K_1)$ versus $1/T$ provides good linearity with a coefficient of determination ($R^2 = 0.9659$), which validates the pseudo-first-order kinetics presented in Fig. 7. The activation energy (E_a) and Arrhenius constant

Table 2 Pseudo-first-order kinetic data

Temperature (°C)	20	30	40	50
K_1 (min ⁻¹)	0.130	0.238	0.263	0.310
R^2	0.928	0.968	0.99	0.988

(A) value, calculated and noted from the plot $\ln(K_1)$ versus $1/T$ were found to be 23.42 kJ/mol and 2022.32, respectively. The comparative studies of previously reported reaction kinetic constants for the electrochemical & RTB21 removal processes are listed in Table 3. The activation energy mainly depends on the nature of the reaction. The small value of E_a indicates a fast reaction. It is reported in the literature that, for homogeneous diffusion-controlled response $E_a < 40$ kJ/mol, typically in the range of 20 kJ/mol [37–39]. Therefore, the EO process for colour removal of RTB21 in aqueous medium using (rGO/Gr)₂ was more likely of a diffusion-controlled reaction.

3.5 FTIR analysis

Figure 8 represents the FTIR spectrum of graphite powder, GO, rGO. Significant peaks, indicating several functional groups are almost absent in the FTIR spectrum of graphite powder. Only C–H bonds exist at the carbon edges, but in negligible amounts compared to the amounts of C–C/C=C bonds in bulk. A few weak bands can be assigned to adsorbed water molecules. This indicates the chemical inertness of graphite as a bulk material [40].

On the other hand, a perusal of the FTIR spectra of GO indicates the presence of several oxygen-derived species; functional groups in its structure. A highly intense

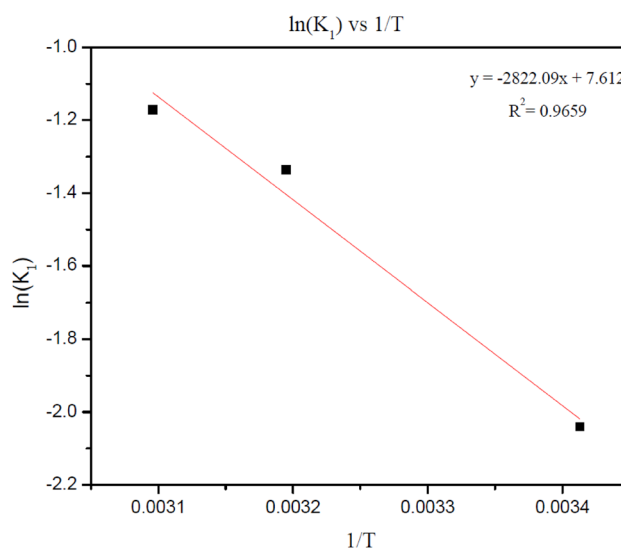
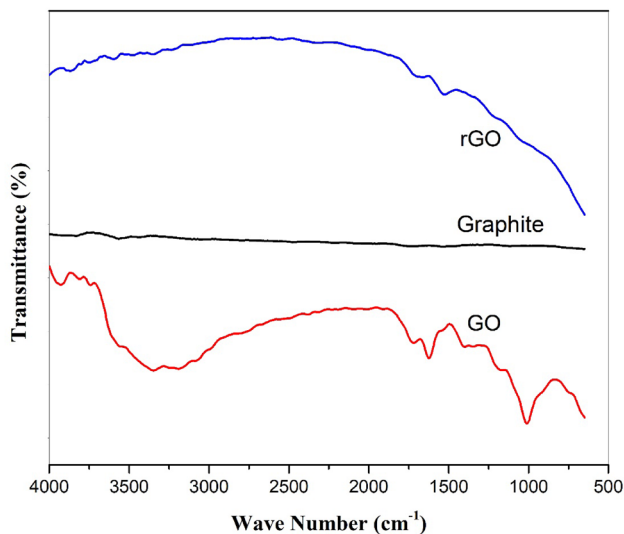


Fig. 7 Plot of $\ln(K_1)$ Vs $1/T$

Table 3 Comparative study of previously reported reaction kinetic constants for electrochemical & RTB21 removal processes

Wastewater	Treatment process (Electrode)	Reaction order (α)	Rate constant (k)	E	A	References
RTB21	Indirect Electro-oxidation Process (rGO/graphite)	1 (p)	0.13–0.31 min ⁻¹	23.42 kJ/mol	2022.32	Present study
4-Chloroguaiacol (4-CG)	Electrochemical oxidation (Nb/PbO ₂)	1 (p)	1.78–4.62 h ⁻¹	15 kJ/mol	–	[37]
Bilgewater	Electrochemical (Pt/Ir)	1	6.775 × 10 ⁻² min ⁻¹	26.2 kJ/mol	1943.0 min ⁻¹	[38]
Phenol	Electrocatalytic (β -PbO ₂)	1 (p)	0.303–1.663 (10 ³ S ⁻¹)	23.8 kJ mol ⁻¹	–	[39]
Beet sugar factory wastewater	Electrocoagulation (Iron)	1.2	0.057 L ^{0.2} /(g ^{0.2} h)	5.17 kJ/mol	0.36 L ^{0.2} /(g ^{0.2} h)	[45]
Resorcinol in the aqueous medium	Electrochemical oxidation (Boron-Doped Diamond Anode)	1	0.0145 min ⁻¹	5.32 kJ/mol and	0.1169 min ⁻¹	[46]
RTB 21	Solar based Photocatalytic	1 (p)	0.0199 min ⁻¹	–	–	[47]
RTB21	Photocatalytic	1 (p)	0.0258 min ⁻¹ (for Nb-TiO ₂) and 0.0225 min ⁻¹ (for Fe: Nb-TiO ₂)	–	–	[48]
RTB21	Pd-catalyzed H ₂ Reduction	1 (p)	0.179 ± 0.009 d ⁻¹	–	–	[49]
RTB21	Adsorption	2 (p)	1.95–6.32 mg g ⁻¹ min ⁻¹	–	–	[50]

(p): pseudo order

**Fig. 8** FTIR spectra of graphite powder, GO, and rGO

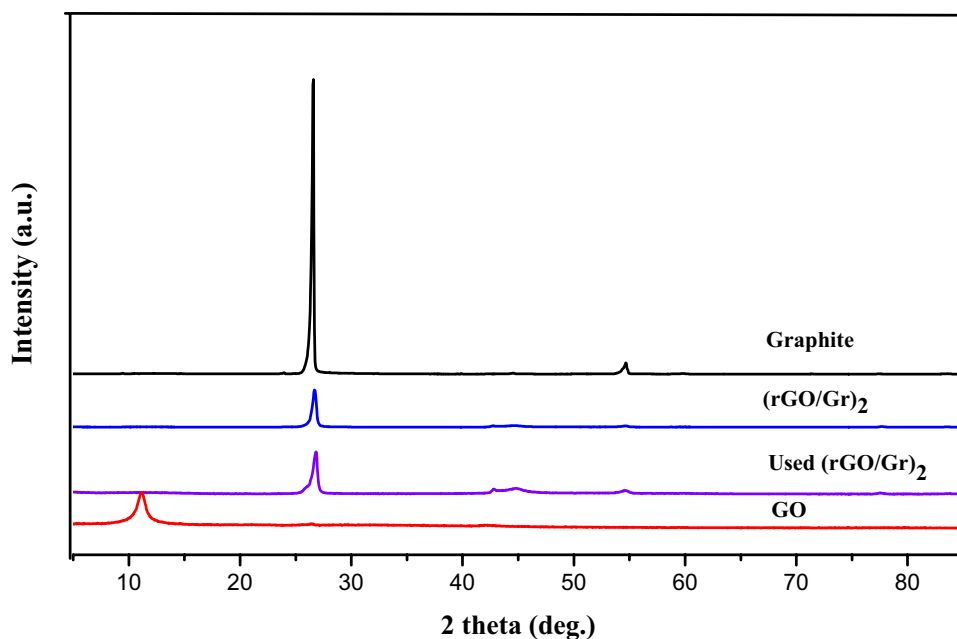
and broad absorption peak at 3350 (2400–3600) cm⁻¹, which corresponds to the O–H stretching vibration, implying the presence of COOH and/or OH functional groups. The bands at 1720, 1631 cm⁻¹ corresponding to C=O stretching (carbonyl group), and C=C stretching, respectively. The bands at 1398 and 1010 cm⁻¹ can be assigned to C–O–C (epoxide group) stretching and C–O stretching (epoxy group), respectively [18]. In essence, the FTIR

results confirmed various oxygen-containing functional groups like hydroxyl, carbonyl, and epoxy, indicating the effective synthesis of GO under present experimental conditions [40]. The FTIR spectra of rGO indicate the absence or weak peaks of oxygenated groups at rGO sheets [18].

3.6 XRD analysis

To analyse the crystallinity of the graphite powder, GO and rGO, the XRD patterns were analysed as shown in Fig. 9. The XRD of the graphite powder shows the presence of sharp and robust peak at $2\theta = 26.53^\circ$ and low-intensity peak at $2\theta = 54.5$, which corresponds to (002) and (004) hkl plane, respectively. It shows high crystallinity of graphite with crystallite size 34.65 nm at 26.53° , calculated by Scherrer's formula [40]. The interlayer spacing was found to be 0.336 nm, calculated by the Bragg's law. For GO, XRD patterns show a peak at $2\theta = 11.1^\circ$ having a hkl plane at (001) with crystallite size 5.17 nm, the interlayer spacing of 0.796 nm. The interlayer spacing of GO increased by 136% compared to graphite power because of oxygenated functional groups present in GO [41]. Almost 85% crystallite size of GO was reduced compared to graphite powder. In the XRD of the (rGO/Gr)₂ electrode surface shows the characteristic peak of rGO at $2\theta = 26.67^\circ$ having a hkl plane at (002) with crystallite size of 17.5 nm and interlayer spacing of 0.334 nm, this was noted for the presence of rGO over graphite surface [18]. The XRD of the used (rGO/

Fig. 9 Wide-angle X-ray diffraction pattern of the graphite flakes, GO powder, and (rGO/Gr)₂ electrode, and used (rGO/Gr)₂ electrode



(Gr)₂ electrode surface after 5 runs shows the characteristic peak of rGO at $2\theta = 26.74^\circ$ with a crystallite size of 14.5 nm and interlayer spacing of 0.333 nm. This indicates good stability of rGO coating over the graphite surface, and it is not leached out into solution.

3.7 FESEM analysis

The morphology of the (a) graphite powder, (b) GO powder, (c) graphite electrode (Gr), (d, e) rGO coated Gr, (f) C/S of rGO coated Gr is illustrated in Fig. 10. The SEM images show the respective sample's surface structures, the synthesized material, and the successful thin coating of rGO over Gr. Stacked layer type structure of graphite powder shown in Fig. 10a. Randomly wrinkled nanosheets of a few micrometer sizes of GO is shown in Fig. 10b, strongly associated with each other by π - π bonds [18]. The FESEM image of the graphite electrode (Fig. 10c) shows the porous structure with a little minor irregularity over the smooth surface significant to a low surface area. From Fig. 10d, e, it is clear that a thin coating of microscale clusters of rGO sheets successfully done over graphite electrode and the average thickness of the coating for (rGO/Gr)₂ is 193.15 μm over Gr (Fig. 10f). However, rGO enhances the overall surface area of the graphite electrode. Hence, the mass transfer rate improves; this can transform into better electrocatalytic performance. The FESEM of used (rGO/Gr)₂ after 5 runs was carried out to check the coating's stability. From Fig. 10g, it shows rGO coating remain present over the Graphite surface, offers good stability of the coating. Actual images of (rGO/Gr)₂ electrode, fresh and used shown in Fig. 10h.

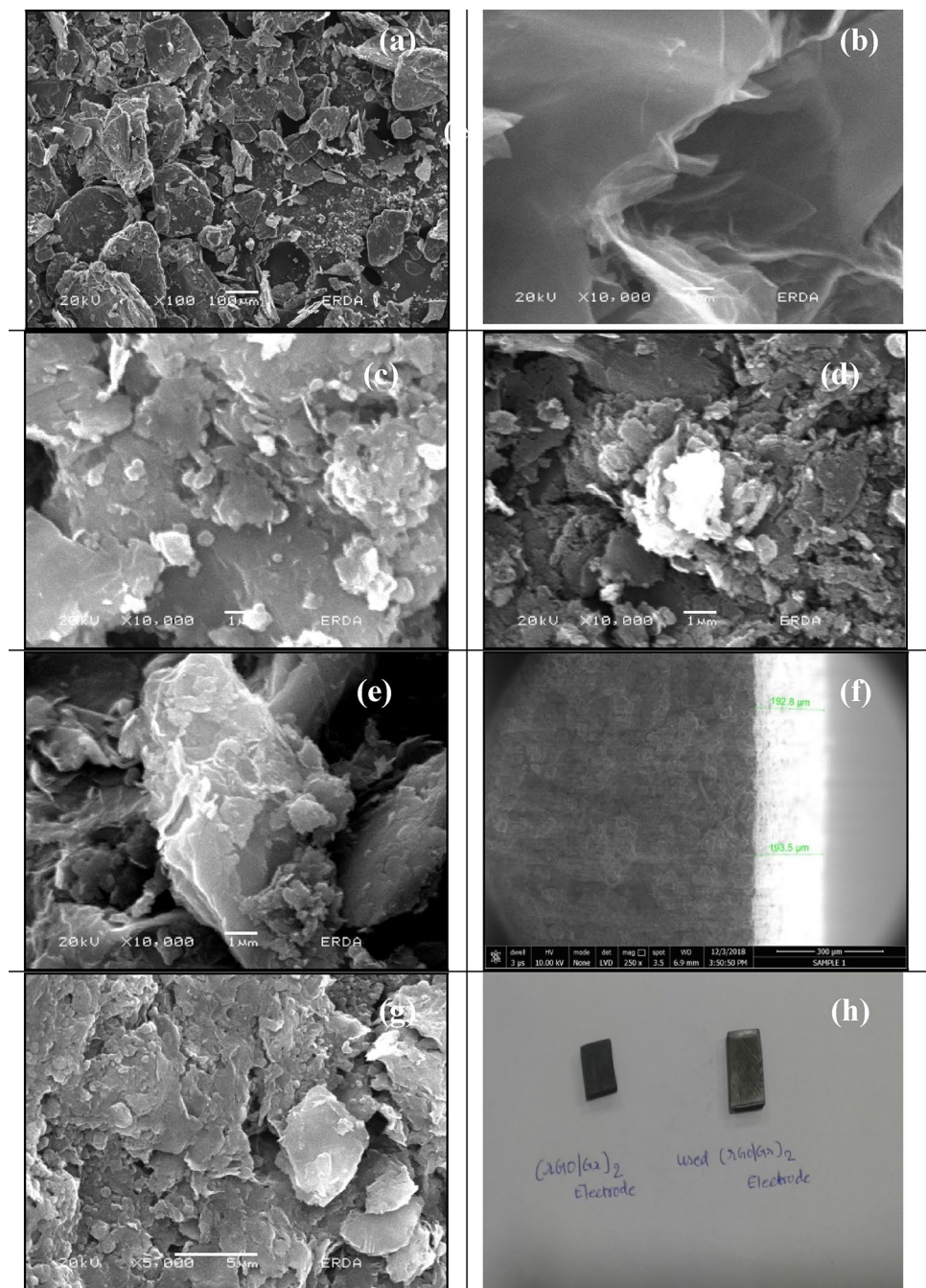
3.8 Contact angle

The contact angle is an essential measure of the wettability of the surface of the graphite electrode. The higher is the contact angle, the lower becomes the tendency to wet the electrode surface with higher hydrophobicity [42]. From Fig. 11, it was observed that the contact angle for graphite electrode (Gr)₀ was 101.55° . The contact angle increased by the coating of rGO over the graphite electrode, having value 109.85° and 112.3° for (rGO/Gr)₁ and (rGO/Gr)₂, respectively, shows that the hydrophobicity of the electrode surface-enhanced considerably. As per the literature, the hydrophobicity enhancement indicated that the electrode's stability and catalytic activity improved [43].

3.9 Stability of the coating

The coating's long-term stability is also an important performance index for the electrochemical process to treat wastewater and future environmental applications [44]. Therefore, to check the coating's stability, the electro-oxidation process was repeated 5 times with the same (rGO/Gr)₂ electrode, and the colour removal (%) was observed. The colour removal (%) was dropped from 96.69 to 91.72 after 5 runs. The decline in results can be described by releasing a small amount of rGO diffuse into the water (Fig. 12) [24]. The reason for the electrode's prolonged service life may be due to the improvement in hydrophobicity of the coated electrode [43]. The FESEM and XRD of used (rGO/Gr)₂ electrode also represent the coating's

Fig. 10 FESEM micrographs of graphite power (a), GO (b), the surface of (Gr)₀ (c), the surface of (rGO/Gr)₁ (d), the surface of (rGO/Gr)₂ (e), the cross-section of (rGO/Gr)₂ (f), the surface of used (rGO/Gr)₂ (g), actual images of (rGO/Gr)₂ electrode, fresh and used (h)



good stability. However, improvement in the stability of the coating could be the future scope of research.

4 Conclusions

The colour removal efficiency of the indirect electro-oxidation process for synthetic RTB21 dye wastewater was improved by modification of the surface of the graphite electrode using dip-coating of GO and reduced to rGO by a thermal method. GO was successfully synthesized

using improved Hummer's method. The resultant graphite electrode, designated as (Gr)₀, (rGO/Gr)₁, and (rGO/Gr)₂, were examined by using FTIR, XRD, FESEM, and Contact Angle. FTIR and XRD analysis indicate that GO was successfully synthesized and coated over the pre-treated graphite electrode. The results of the electro-oxidation process were analysed with respect to the effect of operating process parameters such as current density (A/m²), initial pH, NaCl as electrolyte concentration (g/L), and temperature (°C). Per cent colour removal was improved by 10.5% and 25.80% using a modified

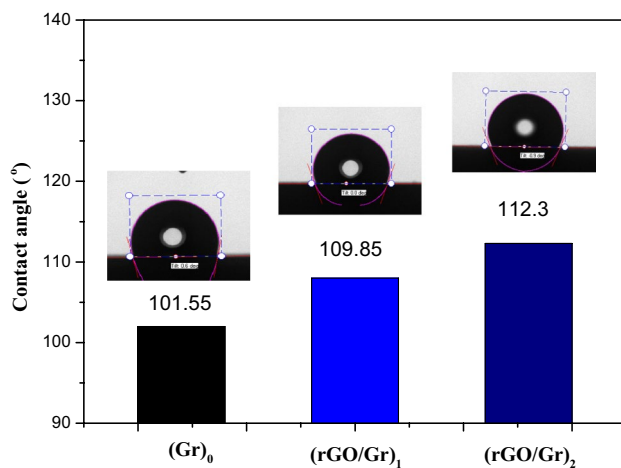


Fig. 11 Contact angle for (Gr)₀, (rGO/Gr)₁, and (rGO/Gr)₂

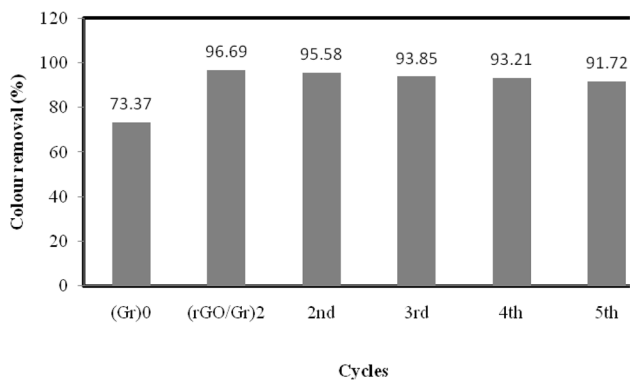


Fig. 12 Stability of the (rGO/Gr)₂ over 5 cycles. Conditions: 7 pH, 200 A/m² current density, 2 g/L NaCl concentration, 30 °C temperature, and 15 min process time

graphite electrode (rGO/Gr)₁ and (rGO/Gr)₂, respectively, at 50 ppm RTB21 dye concentration, 7.0 initial pH, 200 A/m², 2 g/L NaCl concentration, 30 °C temperature, and 15 min process time. The RTB21 decolourization by the indirect electro-oxidation process followed the pseudo-first-order kinetics, and the activation energy and Arrhenius constant (*A*) value were estimated to be 23.42 kJ/mol, and 2022.32, respectively.

The data obtained in the present study could be used as guidelines for the design and scale up of the electro-oxidation unit for possible commercial applications.

Acknowledgements The authors are grateful for the support to carry out analyses provided by the Shah-Schulman Centre for Surface Science and Nanotechnology (SSCSSN), Nadiad, Sophisticated Instrumentation Centre for Advance Research & Testing (SICART), Vallabh Vidyanagar, and the Electrical Research and Development Association (ERDA), Vadodara.

Compliance with ethical standards

Conflict of interest Authors have no conflict of interest.

References

- Li S, Wang L, Yang X, Wang Y (2017) Activated carbon produced from sugarcane bagasse waste as a low-cost dye-containing wastewater adsorbent for reactive turquoise blue removal. *Desalination Water Treat* 81:315–321. <https://doi.org/10.5004/dwt.2017.21105>
- Liu S, Li B, Qi P, Yu W, Zhao J, Liu Y (2019) Performance of freshly generated magnesium hydroxide (FGMH) for reactive dye removal. *Colloids Interface Sci Commun* 28:34–40. <https://doi.org/10.1016/j.colcom.2018.11.004>
- Bilińska L, Blus K, Gmurek M, Ledakowicz S (2019) Coupling of electrocoagulation and ozone treatment for textile wastewater reuse. *Chem Eng J* 358:992–1001. <https://doi.org/10.1016/j.cej.2018.10.093>
- Gangwar R, Rasool S, Mishra S (2016) Evaluation of cellobiose dehydrogenase and laccase containing culture fluids of *Termitomyces* sp. OE147 for degradation of Reactive blue 21. *Biotechnol Rep* 12:52–61. <https://doi.org/10.1016/j.btre.2016.10.002>
- Can OT, Bayramoglu M, Kobya M (2003) Decolorization of reactive dye solutions by electrocoagulation using aluminum electrodes. *Ind Eng Chem Res* 42:3391–3396. <https://doi.org/10.1021/ie020951g>
- Suen NT, Hung SF, Quan Q, Zhang N, Xu YJ, Chen HM (2017) Electrocatalysis for the oxygen evolution reaction: recent development and future perspectives. *Chem Soc Rev* 46:337–365
- Daneshvar N, Behnajady MA, Mohammadi MKA, Dorraji MSS (2008) UV/H₂O₂ treatment of Rhodamine B in aqueous solution: influence of operational parameters and kinetic modeling. *Desalination* 230:16–26. <https://doi.org/10.1016/j.desal.2007.11.012>
- Farhadi S, Aminzadeh B, Torabian A, Khatibikamal V, Fard MA (2012) Comparison of COD removal from pharmaceutical wastewater by electrocoagulation, photoelectrocoagulation, peroxi-electrocoagulation and peroxi-photoelectrocoagulation processes. *J Hazard Mater* 219–220:35–42. <https://doi.org/10.1016/j.jhazmat.2012.03.013>
- Khandegar V, Saroha AK (2013) Electrocoagulation for the treatment of textile industry effluent—a review. *J Environ Manag* 128:949–963
- Sandhwar VK, Prasad B (2017) Comparative study of electrochemical oxidation and electrochemical Fenton processes for simultaneous degradation of phthalic and para-toluic acids from aqueous medium. *J Mol Liq* 243:519–532. <https://doi.org/10.1016/j.molliq.2017.08.016>
- Panizza M, Cerisola G (2007) Electrocatalytic materials for the electrochemical oxidation of synthetic dyes. *Appl Catal B Environ* 75:95–101. <https://doi.org/10.1016/j.apcatb.2007.04.001>
- Rivera M, Pazos M, Sanromán MÁ (2011) Development of an electrochemical cell for the removal of Reactive Black 5. *Desalination* 274:39–43. <https://doi.org/10.1016/j.desal.2011.01.074>
- Kariyajanavar P, Jogtappa N, Nayaka YA (2011) Studies on degradation of reactive textile dyes solution by electrochemical method. *J Hazard Mater* 190:952–961. <https://doi.org/10.1016/j.jhazmat.2011.04.032>
- Qiao MX, Zhang Y, Zhai LF, Sun M (2018) Corrosion of graphite electrode in electrochemical advanced oxidation processes: Degradation protocol and environmental implication. *Chem Eng J* 344:410–418. <https://doi.org/10.1016/j.cej.2018.03.105>

15. Bondarenko EA, Mazanik AV, Streltsov EA, Kulak AI, Korolik OV (2015) SnO₂/reduced graphene oxide composite films for electrochemical applications. *Mater Sci Eng B* 202:61–67. <https://doi.org/10.1016/j.mseb.2015.10.002>
16. Mousset E, Ko ZT, Syafiq M, Wang Z, Lefebvre O (2016) Electrocatalytic activity enhancement of a graphene ink-coated carbon cloth cathode for oxidative treatment. *Electrochim Acta* 222:1628–1641. <https://doi.org/10.1016/j.electacta.2016.11.151>
17. Li Y, Han J, Xie B, Li Y, Zhan S, Tian Y (2017) Synergistic degradation of antimicrobial agent ciprofloxacin in water by using 3D CeO₂/RGO composite as cathode in electro-Fenton system. *J Electroanal Chem* 784:6–12. <https://doi.org/10.1016/j.jelechem.2016.11.057>
18. AkerdiEs'haghzadeBahramiArami AGZSHM (2017) Comparative study of GO and reduced GO coated graphite electrodes for decolorization of acidic and basic dyes from aqueous solutions through heterogeneous electro-Fenton process. *J Environ Chem Eng* 5:2313–2324. <https://doi.org/10.1016/j.jece.2017.04.028>
19. Li G, Xia Y, Tian Y, Wu Y, Liu J, He Q, Chen D (2019) Review—recent developments on graphene-based electrochemical sensors toward nitrite. *J Electrochem Soc* 166:B881–B895. <https://doi.org/10.1149/2.0171912jes>
20. Li Q, Xia Y, Wan X, Yang S, Cai Z, Ye Y, Li G (2020) Morphology-dependent MnO₂/nitrogen-doped graphene nanocomposites for simultaneous detection of trace dopamine and uric acid. *Mater Sci Eng C* 109:110615. <https://doi.org/10.1016/j.msec.2019.110615>
21. Cai Z, Ye Y, Wan X, Liu J, Yang S, Xia Y (2019) Morphology—dependent electrochemical sensing properties of iron oxide—graphene oxide nanohybrids for dopamine and uric acid. *Nanomaterials* 835:1–19
22. Li G, Wu J, Jin H, Xia Y, Liu J, He Q, Chen D (2020) Titania/electro-reduced graphene oxide nanohybrid as an efficient electrochemical sensor for the determination of allura red. *Nanomaterials* 10:1–15. <https://doi.org/10.3390/nano10020307>
23. Wan X, Yang S, Cai Z, He Q, Ye Y, Xia Y, Li G, Liu J (2019) Facile synthesis of MnO₂ nanoflowers/N-doped reduced graphene oxide composite and its application for simultaneous determination of dopamine and uric acid. *Nanomaterials* 9:1–16. <https://doi.org/10.3390/nano9060847>
24. Zhang Z, Meng H, Wang Y, Shi L, Wang X, Chai S (2018) Fabrication of graphene@graphite-based gas diffusion electrode for improving H₂O₂ generation in electro-Fenton process. *Electrochim Acta* 260:112–120. <https://doi.org/10.1016/j.electacta.2017.11.048>
25. Aksu Z, Isoglu IA (2007) Use of dried sugar beet pulp for binary biosorption of Gemazol Turquoise Blue-G reactive dye and copper (II) ions: equilibrium modeling. *Chem Eng J* 127:177–188. <https://doi.org/10.1016/j.cej.2006.09.014>
26. Vaghela NR, Nath K (2019) Reclamation of model wastewater containing Rhodamine B by electrochemical Fenton (ECF) process. *J Sci Ind Res* 78:624–628
27. Kang JH, Yoon Y, Song JH (2020) Effects of pH on the simultaneous removal of hydrogen sulfide and ammonia in a combined absorption and electro-oxidation system. *J Hazard Mater* 382:121011. <https://doi.org/10.1016/j.jhazmat.2019.121011>
28. Nandi BK, Patel S (2017) Effects of operational parameters on the removal of brilliant green dye from aqueous solutions by electrocoagulation. *Arab J Chem* 10:S2961–S2968. <https://doi.org/10.1016/j.arabjc.2013.11.032>
29. Rajkumar K, Mathkumar M (2017) Statistical optimization of electro oxidation process for removal of textile dye C.I. Reactive Blue 198. *Int J Environ Sci Nat Resour* 1:555570. <https://doi.org/10.19080/ijesnr.2017.01.555570>
30. Tahir H, Shah AR, Iubal S, Kifayatullah H (2017) The statistical optimization of indirect electrochemical oxidation process for the treatment of dye from simulated textile discharge. *Int J Environ Sci Nat Resour* 2:555583. <https://doi.org/10.19080/ijesnr.2017.02.555583>
31. Kariyajanavar P, Narayana J, Nayaka YA (2013) Degradation of textile dye C.I. Vat Black 27 by electrochemical method by using carbon electrodes. *J Environ Chem Eng* 1:975–980. <https://doi.org/10.1016/j.jece.2013.08.002>
32. Rahmani AR, Godini K, Nematollahi D, Azarian G (2015) Electrochemical oxidation of activated sludge by using direct and indirect anodic oxidation. *Desalination Water Treat* 56:2234–2245. <https://doi.org/10.1080/19443994.2014.958761>
33. Sivodia C, Sinha A (2020) Assessment of graphite electrode on the removal of anticancer drug cytarabine via indirect electrochemical oxidation process: kinetics & pathway study. *Chemosphere* 243:125456. <https://doi.org/10.1016/j.chemosphere.2019.125456>
34. Rajkumar K, Muthukumar M (2015) Response surface optimization of electro-oxidation process for the treatment of C.I. Reactive Yellow 186 dye: reaction pathways. *Appl Water Sci* 7:637–652. <https://doi.org/10.1007/s13201-015-0276-0>
35. Duan F, Li Y, Cao H, Wang Y, Crittenden JC, Zhang Y (2015) Activated carbon electrodes: electrochemical oxidation coupled with desalination for wastewater treatment. *Chemosphere* 125:205–211. <https://doi.org/10.1016/j.chemosphere.2014.12.065>
36. Rajkumar D, Palanivelu K (2004) Electrochemical treatment of industrial wastewater. *J Hazard Mater* 113:123–129. <https://doi.org/10.1016/j.jhazmat.2004.05.039>
37. Samet Y, Elaoud SC, Ammar S, Abdelhedi R (2006) Electrochemical degradation of 4-chloroguaiacol for wastewater treatment using PbO₂ anodes. *J Hazard Mater* 138:614–619. <https://doi.org/10.1016/j.jhazmat.2006.05.100>
38. Körbahti BK, Artut K (2010) Electrochemical oil/water demulsification and purification of bilge water using Pt/Ir electrodes. *Desalination* 258:219–228. <https://doi.org/10.1016/j.desal.2010.03.008>
39. Zhou M, Wu Z, Wang D (2002) Electrocatalytic degradation of phenol in acidic and saline wastewater. *J Environ Sci Heal Part A Toxic/Hazardous Subst Environ Eng* 37:1263–1275. <https://doi.org/10.1081/ESE-120005985>
40. Bera M, Chandravati GP, Maji PK (2017) Facile one-pot synthesis of graphene oxide by sonication assisted mechanochemical approach and its surface chemistry. *J Nanosci Nanotechnol* 18:902–912. <https://doi.org/10.1166/jnn.2018.14306>
41. Kartick B, Srivastava SK, Srivastava I (2013) Green synthesis of graphene. *J Nanosci Nanotechnol* 13:4320–4324. <https://doi.org/10.1166/jnn.2013.7461>
42. Elaiassaoui I, Akrouf H, Grassini S, Fulginiti D, Bousselmi L (2019) Effect of coating method on the structure and properties of a novel PbO₂ anode for electrochemical oxidation of Amaranth dye. *Chemosphere* 217:26–34. <https://doi.org/10.1016/j.chemosphere.2018.10.161>
43. Li X, Xu H, Yan W (2016) Fabrication and characterization of PbO₂ electrode modified with polyvinylidene fluoride (PVDF). *Appl Surf Sci* 389:278–286. <https://doi.org/10.1016/j.apsusc.2016.07.123>
44. He H, Jiang B, Yuan J, Liu Y, Bi X, Xin S (2019) Cost-effective electrogeneration of H₂O₂ utilizing HNO₃ modified graphite/polytetrafluoroethylene cathode with exterior hydrophobic film. *J Colloid Interface Sci* 533:471–480. <https://doi.org/10.1016/j.jcis.2018.08.092>
45. Güven G, Perendeci A, Tanyolaç A (2009) Electrochemical treatment of simulated beet sugar factory wastewater. *Chem Eng J* 151:149–159. <https://doi.org/10.1016/j.cej.2009.02.008>
46. Körbahti BK, Demirbüken P (2017) Electrochemical oxidation of resorcinol in aqueous medium using boron-doped diamond

- anode: reaction kinetics and process optimization with response surface methodology. *Front Chem* 5:75. <https://doi.org/10.3389/fchem.2017.00075>
47. Bound U, Nanocomposite TO, Vianney YM, Rosalyn I, Angela S (2018) Solar based photocatalytic decolorization of four commercial reactive dyes. *Indones J Chem* 18:621–631. <https://doi.org/10.22146/ijc.27549>
48. Doan NM, Estrellan CR, Purnomo A, Gallardo S, Salim C, Hinode H (2012) Characterization and photocatalytic activity of nano-TiO₂ doped with iron and niobium for turquoise blue dye removal. *AJCHE* 12:34–41
49. Matthews RD, Bottomley LA, Pavlostathis SG (2009) Palladium-catalyzed hydrogen reduction and decolorization of reactive phthalocyanine dyes. *Desalination* 248:816–825. <https://doi.org/10.1016/j.desal.2008.12.043>
50. Yadav A, Mukherji S, Garg A (2013) Removal of chemical oxygen demand and color from simulated textile wastewater using a combination of chemical/physicochemical processes. *I EC Res* 52:10063–10071. <https://doi.org/10.1021/ie400855b>

Publisher's Note Springer Nature remains neutral with regard to jurisdictional claims in published maps and institutional affiliations.